Design and synthesis of two novel carbon aerogels using citric and tartaric acids as catalysts for continuous water desalination

Mohammadreza Alipour[a], Mohamadreza Massoudinejad[a,*], Daryoush Sanaei[a], Hassan Rasoulzadeh[b,*], Mostafa Hadei[c]

[a]*Department of Environmental Health Engineering, School of Public Health and Safety, Shahid Beheshti University of Medical Sciences, Tehran, Islamic Republic of Iran, Tel. +982122432040-1; emails: massoudi2010@yahoo.com/massoudi@sbmu.ac.ir (M. Massoudinejad), mreza.aalipour@gmail.com (M. Alipour), daryss2572@gmail.com (D. Sanaei)*
[b]*Department of Environmental Health Engineering, Student Research Committee, School of Public Health and Safety, Shahid Beheshti University of Medical Sciences, Tehran, Iran, Tel. +989147715780; emails: Hasanrseng@gmail.com/Hrasoulzadeh@sbmu.ac.ir*
[c]*Department of Environmental Health Engineering, School of Health, Tehran University of Medical Sciences, Tehran, Iran, email: mostafa.hadei@gmail.com*

ABSTRACT

This study aimed to find the best capacitive deionization (CD) carbon electrode without supercritical drying by preparing two different types of carbon aerogels with citric (CA) and tartaric (CAS) acid catalysts. Both electrodes were prepared by the short sol–gel process through vacuum drying and pyrolysis with CO_2. The structure, pore size characterization, and electrosorption behavior of electrodes were characterized by scanning electron microscopy (SEM), N_2 adsorption–desorption isotherms, and cyclic voltammetry (CV), respectively. SEM results showed highly porous, smooth, and homogeneous structures without any cracks in both aerogels; however, the two aerogels showed different pore structures. Analysis of the Brunauer–Emmett–Teller surface area also proved no difference between CA and CAS in specific surface area (819 and 636 m^2 g^{-1}, respectively). But the proportion of mesoporosity was higher in CD than CAS; so, CD outperformed CAS. CV also showed better capacitive behavior than CAS since CAS needed more potential. The performance of CD was considered in different concentrations of NaCl aqueous solutions (range: 200–1,000 mg L^{-1}) and at various applied voltages (range: 0.8–2 V). Besides, results revealed that salt-adsorption for CA and CAS in optimum NaCl concentration of 250 mg L^{-1} and applied voltage of 2 V was 22.4 and 12.8 mg g^{-1}, respectively.

Keywords: Carbon aerogel; Citric and tartaric acids; Brackish water; Desalination

1. Introduction

Developing desalination technologies is a certain requirement even in water-rich countries due to the increasing rate of population growth, industrialization, as well as a shortage of freshwater. For the last decades, reverse osmosis (RO) [1], Thermal technologies [2] and ion-exchange (IX) [3] membrane technologies have been the most widely used methods for generating drinking water from the sea and brackish water. RO and thermal technology have been commonly played the main role in producing freshwater, particularly in the Persian Gulf countries [4,5]. These two processes require higher energy consumption and operational costs [6]. Compared to these two techniques, control capacitive deionization (CD) has reduced the cost of energy consumption because of low scaling and fouling. It has also

* Corresponding authors.

been shown to be easy to deploy, operate, and maintain [7–9]. CD is an attractive safe (low-pressure and low-voltage) and adequate electrochemical process for brackish water desalination that has received great attention over the past years [10].

A CD cell consists of a pair of porous carbon electrodes, a dielectric separator between the electrodes to preserve the paired electrode from electrical short circuits, and current collectors. By applying the electric field by charging voltage between two electrodes, electrical double layers (EDLs) are formed near the electrode and ionic species with an electric charge move to the oppositely charged electrode and are adsorbed. This is known as the electro-sorption process [11]. Thus, for the CD technique, the material and surface area of the electrode are keys to remove ionic constituents from water.

In literature, the effect of electrode type and various carbon materials (graphene [12], activated carbons (AC) [13], carbon nanotubes (CNT) [14], carbon aerogels (CA), (e.g., cryogel, xerogel, and metal oxide doped aerogels), and carbon composites such as ordered-mesopores carbon [15,16]) respectively used in CD cells and in the electrode for deionization performance have been investigated. Among the aforementioned materials, CA with high salt adsorption and electrical conductivity has been considered an ideal electrode for CD [17]. According to previous studies, there are two methods for improving the CA sol–gel and drying process: (1) to decrease polymerization time, and (2) to use ambient drying [18,19]. The preparation of carbon aerogel with acid catalysts accelerates the polymerization in the sol–gel process; hence, we utilized citric and tartaric acids to catalyze the gelling process with no super-critical step and solvent exchange for drying.

Recently, major advances have been made in the flow of feed water to the electrodes for CD cells such as flow-through electrodes [20], flow-between electrodes [21], Fluidized bed electrodes [22], hybrid capacitive deionization (CDI) and desalination battery [23]. These architectural developments for cells have occurred when CD techniques and large-scale CDI desalination modules started to be applied more around the world. However, flow-between electrodes are the most commonly used architectural cells in CD [24].

In this work, we proposed carbon aerogel electrodes consisting of a cationic and anionic capturing electrode appropriate for ion selectivity with different electrode materials. The main aim of the study was to evaluate the CD performance of the developed electrode via vacuum drying for investigating the influence of different charging voltages on NaCl solution during the operation conditions. We also evaluated the efficacy of CD performance in laboratory-scale tests.

2. Materials and methods

2.1. Materials

Resorcinol (R) >99% and an aqueous solution of formaldehyde (F) (37%wet, with 10% methanol) were supplied from Merck, Germany. Ethanol and acetone (pure, technical grade) solutions were also purchased from Sigma Aldrich, Germany. Further, citric and tartaric acids (C, 1.0 N; standardized solution) were obtained from Merck, Germany.

Besides, for carbon aerogels synthesis, deionized water (W) and sealable containers for gelation (200 mL, polypropylene with screw cap) were used.

2.2. Synthesis of organic gels, drying and pyrolysis

In this study, the molar ratios used for the synthesis of resorcinol–formaldehyde gels were 0.5, 250, and 0.02 for R:F, R:C, and R:W, respectively. For each sample, resorcinol was dissolved in deionized water at room temperature (23°C–25°C). Then, aqueous formaldehyde was added gradually and the solutions were stirred for 10 min to obtain homogeneous solutions. Tartaric and citric acid 1N were added to the solutions as catalysts until their pH was fixed at 3.5 and 5.5, respectively and the resulting suspension was stirred for another 20 min at 600 rpm by a magnetic stirrer. Then, the resulting colorless solution was divided between two sealable polypropylene containers.

At gelation time of RF aerogels, samples with citric acid (CA) and tartaric acid (CAS) were put in an oven for 2 and 1 h, respectively at 95°C. After polymerization, without any solvent exchange, the gels and just two times washing with ethanol and acetone, cut to defined size (1 cm × 4 cm × 3 cm) and dried at –0.04 MPa and 110°C in a vacuum drying chamber (OV-12, Jiao Tech, Seoul, Korea) for 24 h. After 3 h, the carbon aerogels were provided by carbonizing at 950°C in an inert atmosphere of CO_2 gas.

2.3. Cell preparation and lab bench-scale CD

Each aerogel sheet had an approximate density of 0.5 g cm^{-3}. The aerogel sheets were then connected to titanium sheets as a current collector by a copper conductive adhesive. Next, the bonding areas of the electrode and titanium plate were covered with silicone adhesive to prevent the oxidation of the copper adhesive by air. As presented (Fig. S1), a current collector was connected to the copper wire by double-ended alligator electric cables to provide a connection to a DC power supply for stabilizing and changing the voltage. Accordingly to Fig. 1a, the CD cell consists of a pair of an electrode placed in a Plexiglas housing by bolts and nuts and the distance between the electrodes was adjusted to 3 mm. As shown in Fig. 1b, the diagrammatic sketch of the CD test, the lab-scale system includes a digital conductivity meter, peristaltic pump, power supply, and CD unit. NaCl solutions experimented during this work was obtained from the equation and calibration curve derived from seven tests presented (Fig. S2). Synthetic NaCl solutions employed as feed flow with a rate of 50 ml min^{-1} was fed into a CD. The conductivities of these brackish solutions (200, 500 and 1,000 μS cm^{-1}) and the treated water samples were measured by conductivity meter in one cycle. In the present study, the specific electrosorption capacity was defined as Eq. (1) [25]:

$$\left(\frac{mg}{g}\right) = \frac{(C_i - C_e)V}{m} \tag{1}$$

where C_i and C_e are the initial and final concentrations, respectively, V is the volume of the saline solution, and m is the quantity of carbon electrode.

2.4. Characterization

The surface structure and morphology of the carbon aerogels were analyzed by scanning electron microscopy (SEM, SU3500 Hitachi, Japan). The surface area, pore-volume, and pore size distributions were estimated by using the Brunauer–Emmett–Teller (BET) and Barrett–Joyner–Halenda (BJH) methods, respectively. The *t*-plot analysis was also used to analyze the mesopores area as well as microspores volumes. Raman Spectrometer (MultiRAM, Bruker Company, USA) of both carbon electrodes were analyzed in a range of wavelengths from 500 to 3,500 cm with an argon-ion laser. Moreover, to analyze the composition and chemistry of the electrodes, the X-ray photoelectron spectroscopy (XPS) was applied with an Al X-rays micro-focused monochromator (K-alpha, Thermo Fisher Scientific Company, USA). The electrosorption was also carried out at room temperature and cyclic voltammetry (CV) was measured at various scan rates in the potential range from –0.8 V to 0.2 V in 1 M NaCl. Furthermore, electrical specific conductance was measured for both CA and CAS by using the four-point probe method (DEP-02, SES Instruments & Pvt. Ltd., India). Also, Ag/AgCl (Silver/Silver Chloride Electrode, 3.5 M KCl) and platinum were used as reference electrode and counter electrode, respectively. Besides, the specific capacitance was calculated from the CV curves on the basis of the following equation [26]:

$$C = \frac{Q}{\Delta V m} \tag{2}$$

where Q is the average charge, m is the mass of active material in grams, ΔV is the potential window, and C (F g^{-1}) is the specific capacitance.

3. Results and discussion

3.1. SEM morphologies of carbon aerogel samples

Figs. 2a and b show the SEM micrographs of the CA and CAS. As can be seen, both carbon aerogels have highly porous and three-dimensional network structures. Because of the high velocity of sol–gel at the low pH in the polymerization process, aggregation of monomers occurred and large microspheres particles with homogenous size were shaped, which is obvious at a magnification of Figs. 2a and b. The acid-catalyzed sol–gel particles have a thin neck, which can be related to the effects of the short aging time and nucleophilic attack of acid-catalyst [27,28]. However, the release of carbon dioxide gas due to acid decomposition at low temperatures can lead to the formation of the microspore [18]. The resultant CA and CAS aerogels exhibited a strong particle network with large mesopores and no volume shrinkage microstructure, respectively. Fig. 2a shows the large mesopores and microspores, while in Fig. 2b several mesopores can be observed at the surface of the CAS.

3.2. Pore characteristics of CA and CAS

The porous property of CA and CAS were investigated by low-temperature N_2 adsorption–desorption tests. The N_2 adsorption–desorption isotherms and the Barrett–Joyner–Halenda methods used for the pore size distribution of CA and CAS are shown in Figs. 2c and d, respectively. The isotherms of CA and CAS can be classified as type I and IV, according to the International Union of Pure and Applied Chemistry classification. Fig. 3a shows hysteresis loops at relative pressures higher than 0.7 for CA indicating the presence of a large quantity of mesopores, while CAS has the main microspores structure with no mesopores area. This is presumably due to the poor structure of CAS, which caused some mesopores to collapse to other pores during pyrolization [27]. Therefore, we can claim that the presence of both mesopores and microspores in an ideal carbon material is required for appropriate CD performance. Mesopores can provide proper transport for ions to the surface of carbon material to developing the electric double layer, while microspores with many channels are suitable for permeation of electrolyte [29]. CA in Fig. 2c shows a microspores structure and predominant mesopores with competent pore size distributions that play an essential role in the ideal CD process. Also, curves (c) and (d) in Fig. 2 indicate

(a)   (b)
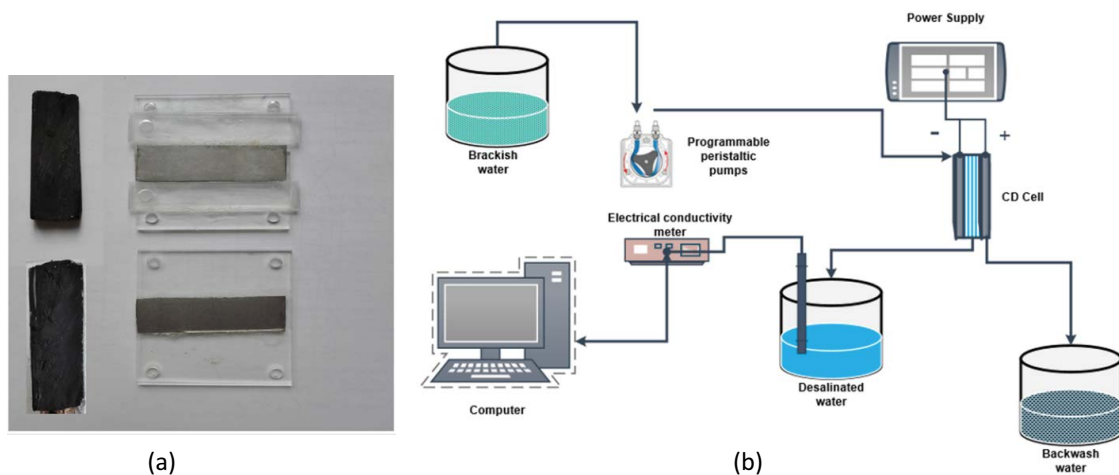
Fig. 1. (a) A cell and electrodes for capacitive deionization and (b) flow schematic of CD pilot-scale experiment system.
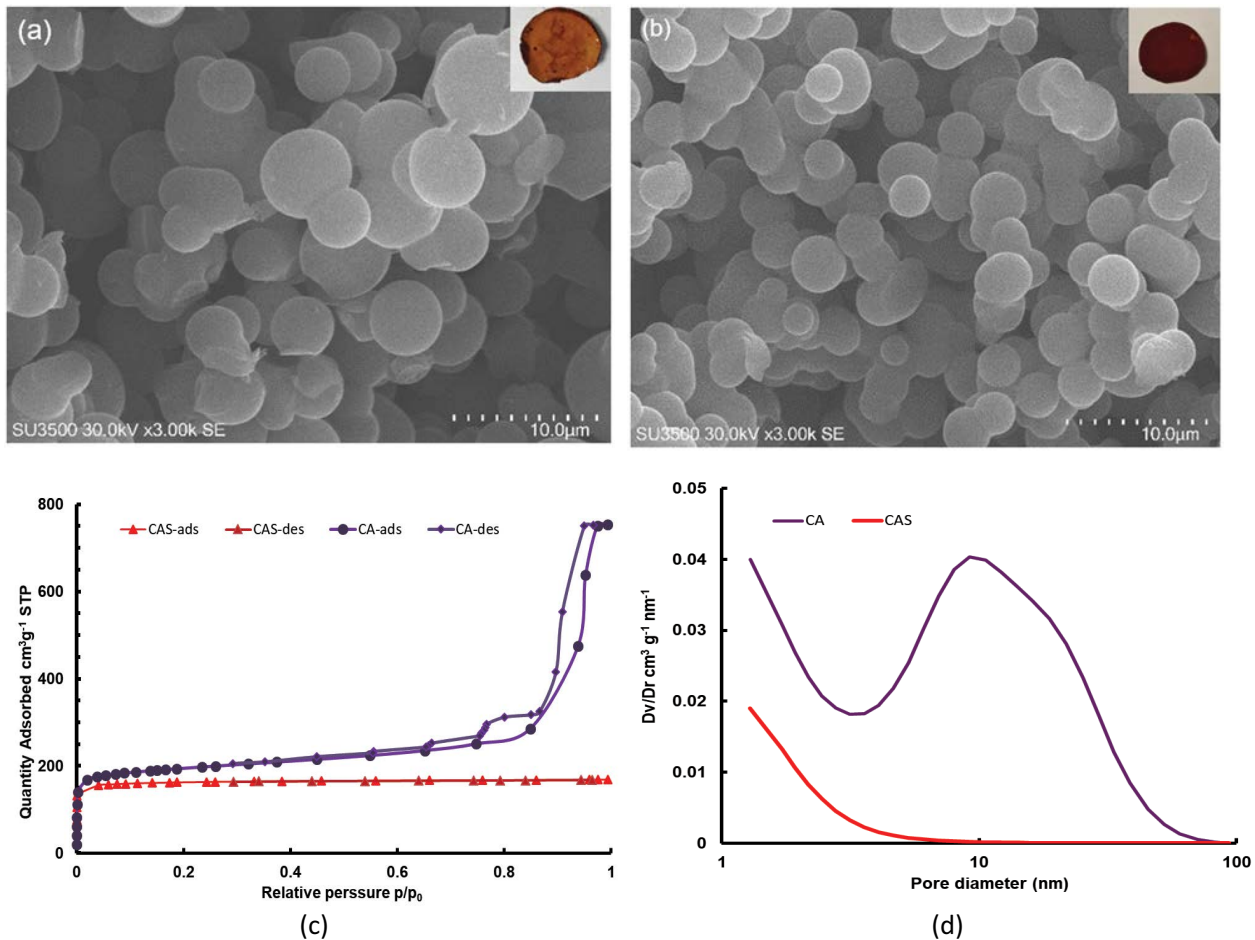
Fig. 2. SEM images of (a) CA, (b) CAS, (c) N_2 adsorption–desorption isotherms and (d) BJH pore size distribution of CA and CAS.

that the CAS produced by vacuum drying had microspores structure with approximately 819 m² g⁻¹ specific area while having an unfavorable pore size distributions. Table 1 presents the BET specific surface area and Pore properties of CA and CAS.

In the CD process, one of the removal characteristics is typically related to the radius of hydrated ions with ionic conductivity, which is 0.35 nm and 50.1 S cm² mol⁻¹ for Na and 0.33 nm with 76.3 S cm² mol⁻¹ for Cl, respectively [30]. As shown in Table 1, the average pore diameters for CA and CAS are 6.5 and 1.5 nm, respectively, so that the largest pores of CA and a small part of CAS pores are larger than the ionic radius.

3.3. XPS and Raman spectra characterization of carbon electrodes

In the current work, to further characterization of electrode structure, Raman spectroscopy was performed for both CA and CAS (Fig. S3). Two particular emerged peaks in each graph correspond to the D and G bands. Revealed D bands in CA and CAS at around 1,355 and 1,340 cm⁻¹, respectively was related to the disordered carbon structure. The G band in CA and CAS observed at about 1,585 and 1,570 cm⁻¹ was attributed to the graphitic composition of samples. In addition, 2D-bands for CA and CAS at 2,800 cm⁻¹ are illustrated

Table 1
Pore characteristic of CA and CAS aerogels

	CA	CAS
S_{BET} (m² g⁻¹)	819	636
r_p peak (nm)	7.98	1.29
V_p (cm³ g⁻¹)	0.96	0.02
V_{total} (cm³ g⁻¹)	164	146
Average pore diameter (nm)	6.5	1.5

in Fig. S3. In spectroscopy, due to 2D-bands, the high-temperature of pyrolysis with CO_2 caused graphite structure as it was expected.

Towards a better understanding of elemental composition and the overall electronic structure, the main compositions of electrodes were analyzed by XPS. The curves of both CA and CAS are shown in Fig. 3. As shown, the particular components in both electrodes are oxygen and carbon. The observed C1s spectrums in Fig. 3 include two peaks for each carbon electrode at 287.5, 287, 288.5, and 287.4 eV for CA and CAS, respectively. We found that these peaks related to the carbon in CA and CAS occur principally as C–O and C=O. The peaks at 284.8 and 285 eV were referred
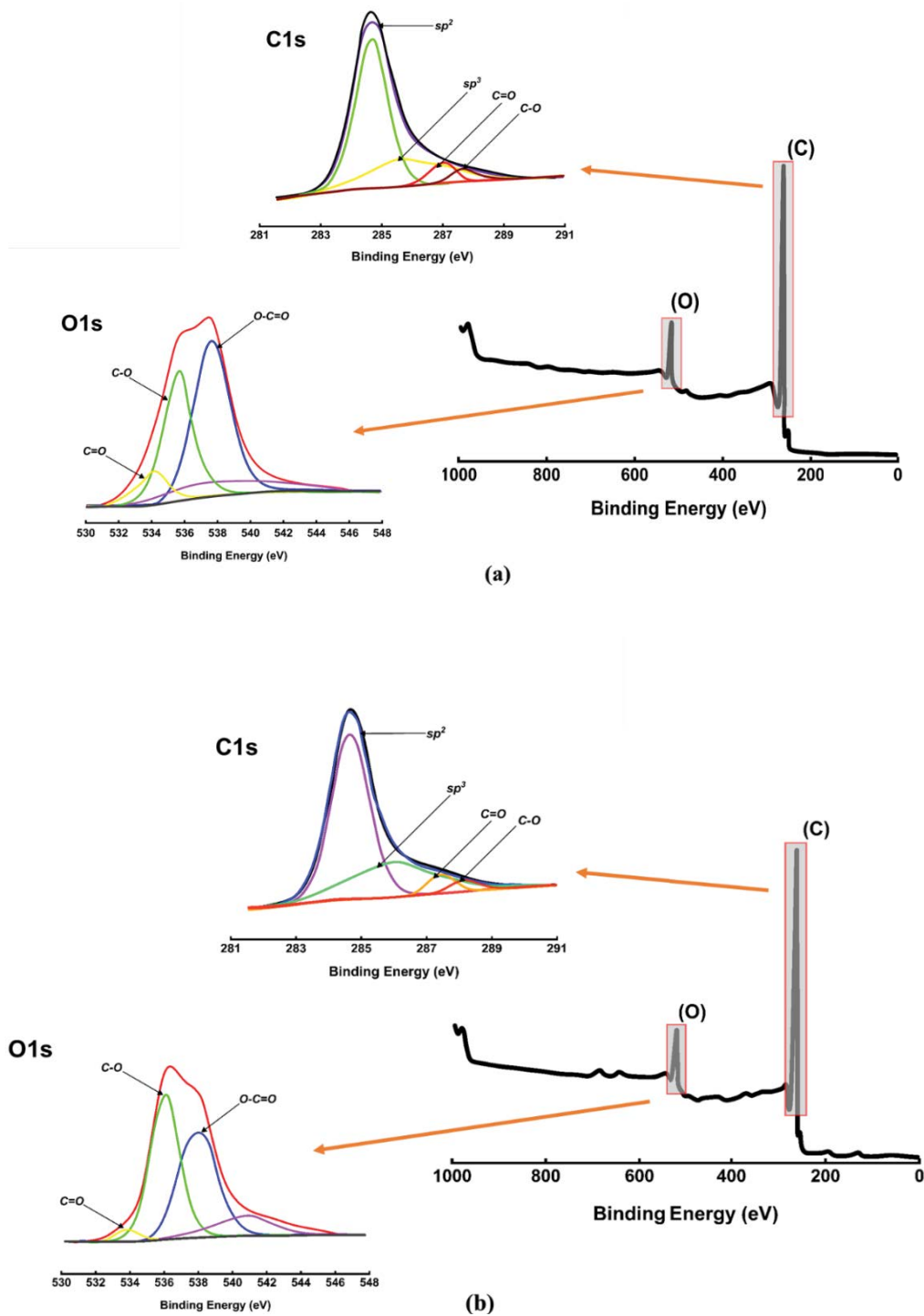
Fig. 3. X-ray photoelectron spectra of carbon aerogel electrodes.

to the C=C bands in CA and CAS related to the graphitic nature of samples shown as sp² in Fig. 3. The peaks at 285.8 and 286.4 eV also indicated the C–C bands (sp³), which were linked to the disordered structure of the samples. As shown in Fig. 3, the O1s spectrums have three peaks at 534 and 533.8 eV as C=O, 535.7 eV and 536 eV as C–O, and 538 and 538.3 eV as O–C=O.

3.4. Capacitance measurements

Electrosorption characterization was measured at room temperature in a typical four-electrode probe experiment performed for both CA and CAS electrode. As shown in Figs. 4a and b, for obtaining the one current density, CAS needs higher potential, while CA has better electrical conductivity behavior. The lower conductivity of
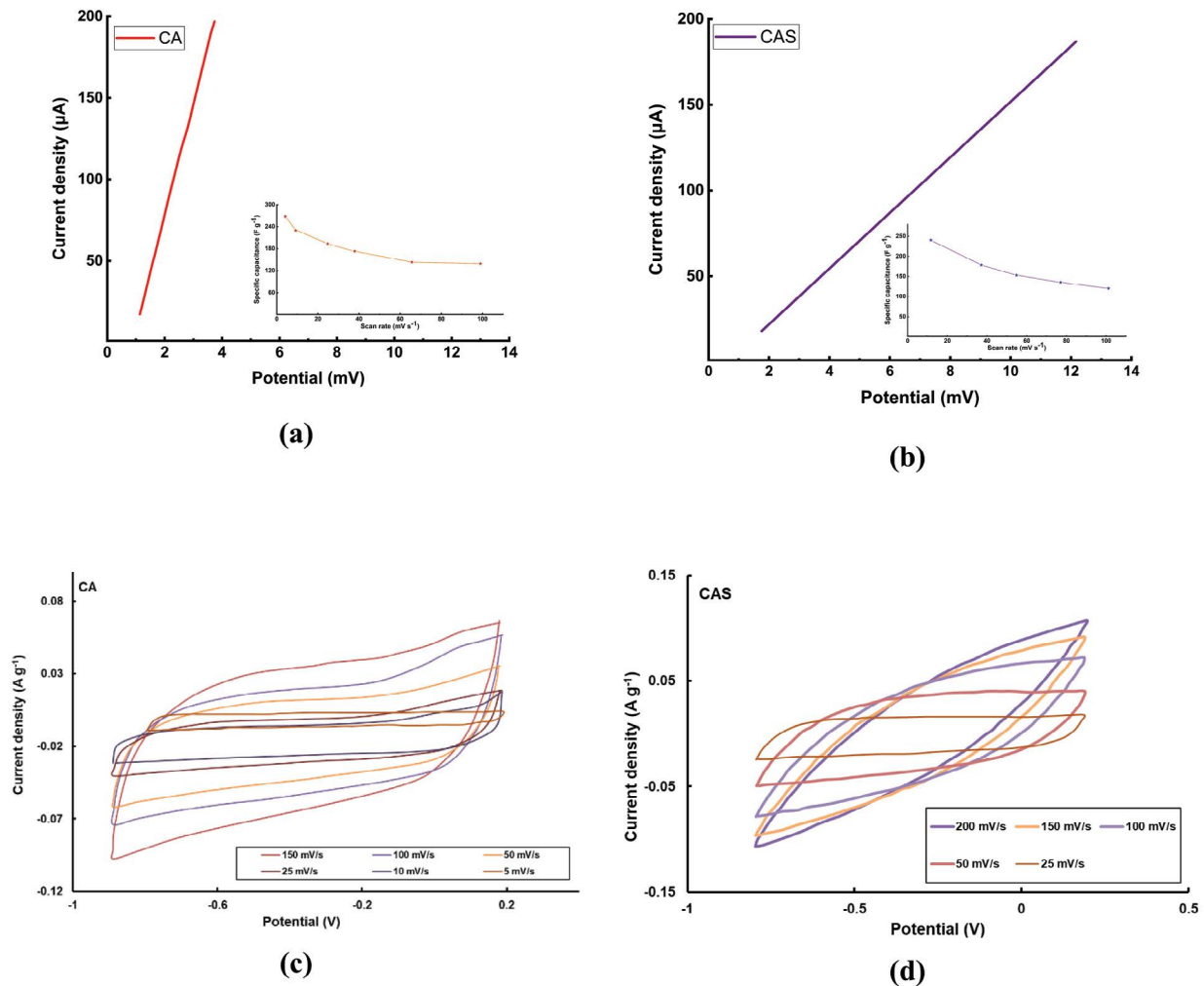
Fig. 4. (a and b) Electrical conductivity and the specific capacitance by scan rate of CA and CAS. (c and d) Cyclic voltammetry of CA and CAS.

CAS was probably related to its Impenetrable structure. The electrical conductivity for CA and CAS electrodes was measured as 3.4 and 59 Sm⁻¹, respectively. Furthermore, the CV curves of the CA and CAS electrodes were measured in 1 M NaCl solution with a potential of –0.8 to 0.2 V presented in Fig. 4. In this figure, the profiles of CA and CAS curves achieved at scan rates ranged between 5–150 mVs⁻¹ and 25–200 mVs⁻¹, respectively. In Fig. 4c, it is evident that at low scan rates (5, 10, and 25), the CV curves have an elongated quadrilateral shape due to the pore structure of CA through which the electrolyte can penetrate [31]. With increasing electric current resistance in high scan rates, the ohmic resistance changed the forming behavior of EDL. Then, the curves became deformed to quasi-rectangular. Moreover, the curves were without any redox peaks exhibiting the ideal capacitive performance [32]. This also indicated the cations and anions adsorbed on the surface area of CA via coulombic interaction [33]. According to Fig. 4d, the typical CV curves of the CAS electrode displays a lower voltage range and is approximately less rectangular in shape than the CA electrode. This, indeed,

suggested the inferior electrochemical behavior of CAS electrode. Eventually, the values of specific capacitances were 178 and 58 Fg⁻¹ for CA and 149 and 36 Fg⁻¹ for CAS at 25 and 150 mVs⁻¹ obtained from Eq. (2).

3.5. CD performance of electrodes

The CD behaviors of both carbon electrodes were evaluated by adjusting the applied voltage between 0.8–2 V and the flow rate of solution at 50 ml min⁻¹ at ambient temperature. The concentration of NaCl solution, as the feed stream in all tests, was fixed at 200, 500 and 1,000 µS cm⁻¹. During each test, the carbon electrode was regenerated by replacing the voltage of the electrode and cell rinsed with deionized water. Besides, the timing of shifting voltage to discharging and separating ions from electrodes was considered according to Fig. S4. Under the adsorption and desorption cycles, a digital conductivity meter was used to control any fluctuations in the conductivity of the inlet and outlet stream. Fig. 5a shows the effluent conductivity of the 200 µS cm⁻¹ influent solution in both CA and CAS electrodes with
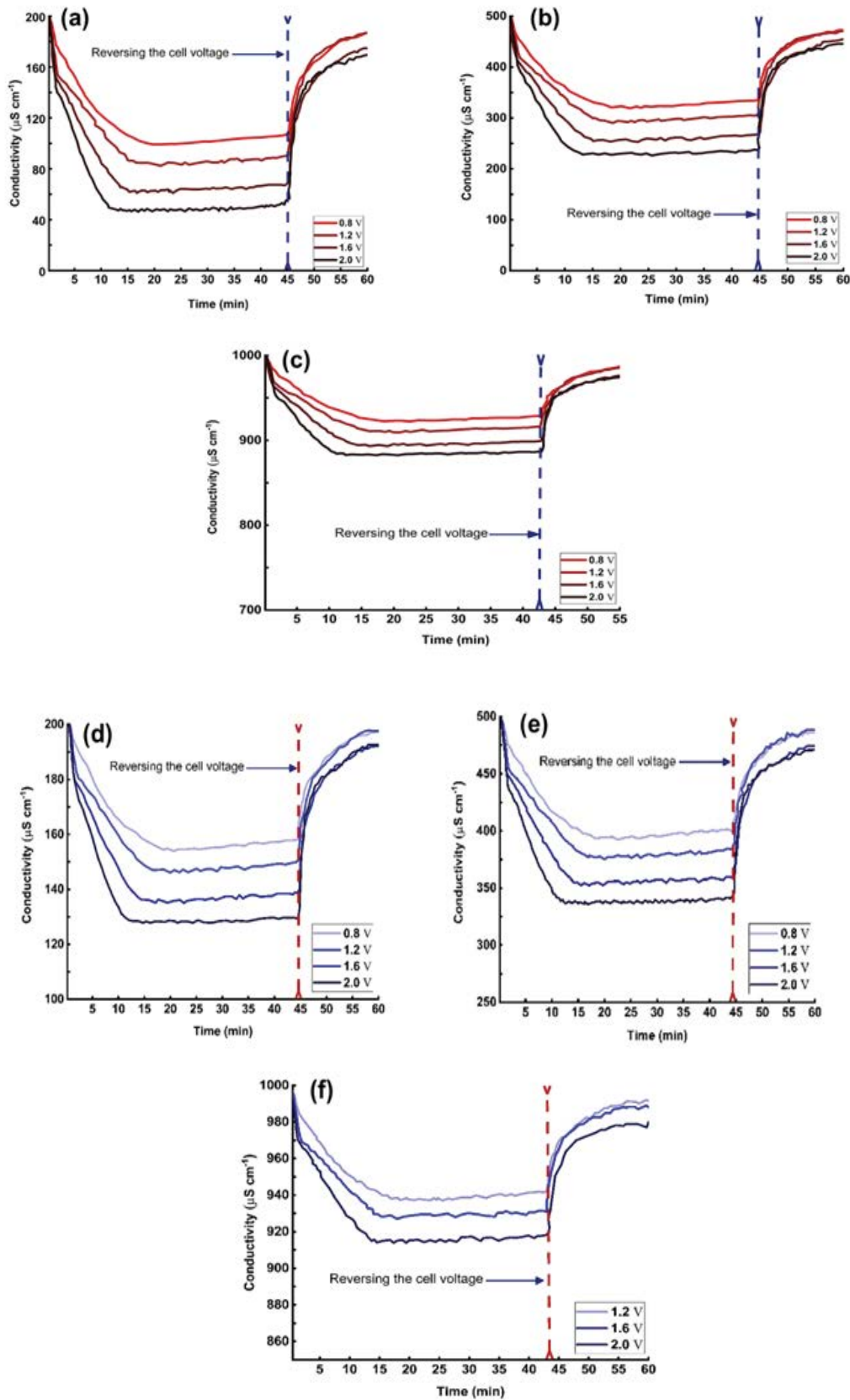
Fig. 5. Variation of NaCl concentration with the applied voltage for CA and CAS. (a) 200 μS cm⁻¹ for CA, (b) 500 μS cm⁻¹ for CA, (c) 1,000 μS cm⁻¹ for CA, (d) 200 μS cm⁻¹ for CAS, (e) 500 μS cm⁻¹ for CAS, and (f) 1,000 μS cm⁻¹ for CAS.

different applied voltages and times. By using NaCl solution as the influent, when the applied voltage to the system increased from 0.8 to 2 V, the NaCl concentration in effluent quickly decreased over time. In all tests, CD cells including CA and CAS electrodes were charged by DC power applied varying voltage, but the current was fixed at 5 A. Figs. 5b and c also show the desalination capacity of CA and CAS at 500 and 1,000 μS cm^{-1} at a different voltage. As expected, the increment of the voltage from 0.8 to 2 V, the removal capacity of the electrodes at both 500 and 1,000 μS cm^{-1} electrolytes also improved. In previously studied adsorption capacities for CD electrodes, when the applied voltage was higher than 1.4 or 1.8 V, the water became hydrolyzed and relatively produced hydrogen and oxygen in the presence of NaCl due to tiny bubbles decrease in the volume of water at higher voltages; hence the process efficiency declined [29,34]. Accordingly, the maximum applied voltage for the prolonged operation in the CD process should be less than 1.3 V [29]. In this study, because of the short operation time of the sorption-desorption cycle of CD cells, no electrochemical decomposition potential was observed by increasing the applied voltage. Therefore, the maximum applied voltage for the CD process was an optimum voltage of 2 V. It is obvious in Fig. 5 that the CAS electrode has lower adsorption capacities rather than CA appropriately matching with the outcomes of N$_2$ adsorption–desorption isotherm and cyclic voltammetry test. Moreover, Fig. 5 represents the comparison between the efficiency of different NaCl concentrations. As seen, the efficiency reduces by an increase in NaCl concentration in both electrodes; although, in 500 mg L^{-1}

concentration, the specific capacity in the CA electrode begins to decrease. However, in all the tests, because of the higher concentration of NaCl, the specific electrosorption capacity increased. The specific electrosorption capacities of CA and CAS electrode at 2 V are shown in Table 2. These amounts are higher than other carbon materials, such as GO [35], AC [36], and G-CNT [37] as an electrode, which are compatible with the related reports. To test the possibility of CA and CAS electrodes application in electrosorption/electrodesorption procedure, we regenerated cycles represented in Fig. 6. In the adsorption process, by changing the positive and negative voltage, the absorbed cations and anions can be desorbed from CA and CAS. Thus, the effluent conductivity immediately rises. Therefore, CD electrodes could be applied either reversibly or stably in adsorption–desorption cycles. In Fig. S5, XPS survey spectra illustrate sodium adsorption for both CA and CAS in adsorption–desorption periods. Materials of the cathode in both electrodes in CA and CAS were determined after five adsorption–desorption cycles and represented Na in 1072 eV. Obviously, due to lack of change in intensity of the electrodes XPS peaks and identical peaks (carbon and oxygen) in adsorption–desorption cycles, oxidation appeared on neither of the cathode electrodes proving that these materials can be applied for several cycles.

4. Conclusion

In summary, CA and CAS performed by short-time polymerization resorcinol and formaldehyde solutions were

Table 2
Ion removal properties and the specific electro sorption capacity

NaCl concentration (mg L^{-1})	Conductivity influent (μS cm^{-1})	Conductivity out (μS cm^{-1}) CA	Conductivity out (μS cm^{-1}) CAS	Time (min)	Q$_{CA}$ (mg g^{-1})	Q$_{CAS}$ (mg g^{-1})
50	106	44	58	40	7.4	6
100	210	101	143	40	12.8	8.2
250	516	325	409	35	22.4	12.8
500	1,030	896	922	30	16	13.3
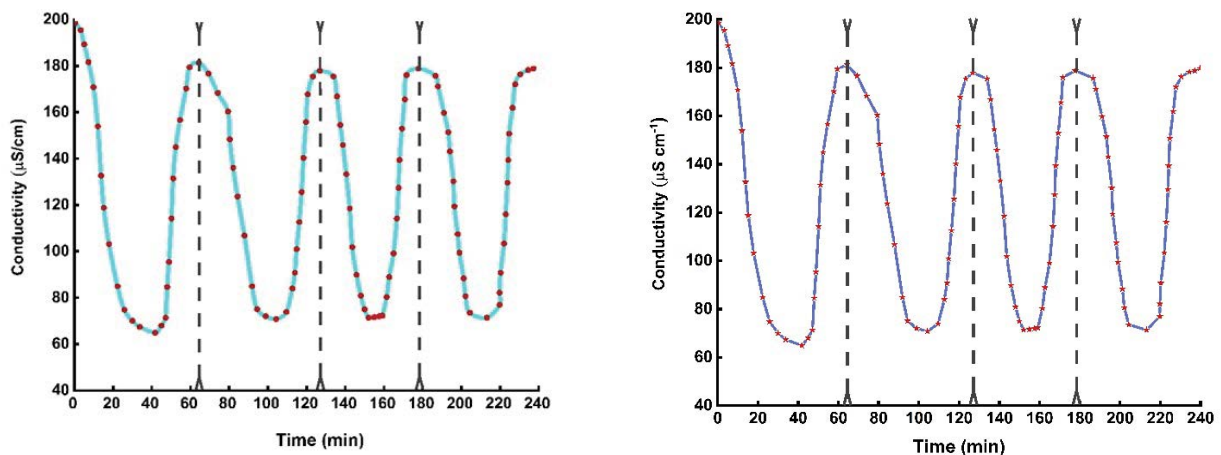
Fig. 6. CA (a) and CAS (b) electrodes performance in several adsorption–desorption cycles.

pyrolyzed under CO_2 atmosphere containing citric and tartaric acid as catalysts and dried by vacuum drying. This method to build CA and CAS electrodes can be easily scaled up for capacitive deionization applications without any cracks and shrinkages on the surface. According to the SEM images, BET analysis, and CV curves of CA and CAS electrodes, to avoid hard costly templates such as supercritical drying to fabricate carbon aerogel, we can achieve a steady structure with desirable conductivity behavior through a simple method. Moreover, the effect of NaCl removal from brackish water by using CA and CAS electrodes was examined and the highest specific electrosorption capacities of CA and CAS occurred in 250 and 500 mg L^{-1} NaCl as well as 22.4 and 13.3 mg g^{-1}, respectively. The designed CA electrode also illustrated great regeneration power and efficiency in several adsorption–desorption cycles.

Acknowledgments

References

[1] A. Subramani, J.G. Jacangelo, Emerging desalination technologies for water treatment: a critical review, Water Res. 75 (2015) 164–187.

[2] M. Chandrashekara, A. Yadav, Water desalination system using solar heat: a review, Renewable Sustainable Energy Rev., 67 (2017) 1308–1330.

[3] H. Yoon, K. Jo, K.J. Kim, J.Y. Yoon, Effects of characteristics of cation exchange membrane on desalination performance of membrane capacitive deionization, Desalination, 458 (2019) 116–121.

[4] M.S. Mohsen, B. Akash, A.A. Abdo, O. Akash, Energy options for water desalination in UAE, Procedia Comput. Sci., 83 (2016) 894–901.

[5] S. Gorjian, B. Ghobadian, Solar desalination: a sustainable solution to water crisis in Iran, Renewable Sustainable Energy Rev., 48 (2015) 571–584.

[6] D. He, C.E. Wong, W.W. Tang, P. Kovalsky, T.D. Waite, Faradaic reactions in water desalination by batch-mode capacitive deionization, Environ. Sci. Technol. Lett., 3 (2016) 222–226.

[7] M.A. Anderson, A.L. Cudero, J. Palma, Capacitive deionization as an electrochemical means of saving energy and delivering clean water. Comparison to present desalination practices: will it compete?, Electrochim. Acta, 55 (2010) 3845–3856.

[8] S. Porada, R. Zhao, A. van der Wal, V. Presser, P.M. Biesheuvel, Review on the science and technology of water desalination by capacitive deionization, Prog. Mater. Sci., 58 (2013) 1388–1442.

[9] S. Sen Gupta, M.R. Islam, T. Pradeep, Chapter 7 – Capacitive Deionization (CDI): An Alternative Cost-Efficient Desalination Technique, S. Ahuja, Ed., Advances in Water Purification Techniques: Meeting the Needs of Developed and Developing Countries, Elsevier, Radarweg 29, P.O. Box: 211, 1000 AE Amsterdam, Netherlands, 2019, pp. 165–202.

[10] M. Wang, X.T. Xu, Y.J. Li, T. Lu, L.K. Pan, Enhanced desalination performance of anion-exchange membrane capacitive deionization *via* effectively utilizing cathode oxidation, Desalination, 443 (2018) 221–227.

[11] M.E. Suss, S. Porada, X. Sun, P.M. Biesheuvel, J. Yoon, V. Presser, Water desalination *via* capacitive deionization: what is it and what can we expect from it?, Energy Environ. Sci., 8 (2015) 2296–2319.

[12] W.Q. Kong, X.D. Duan, Y.J. Ge, H.T. Liu, J.W. Hu, X.F. Duan, Holey graphene hydrogel with in-plane pores for high-performance capacitive desalination, Nano Res., 9 (2016) 2458–2466.

[13] Y.H. Bian, X.F. Yang, P. Liang, Y. Jiang, C.Y. Zhang, X. Huang, Enhanced desalination performance of membrane capacitive deionization cells by packing the flow chamber with granular activated carbon, Water Res., 85 (2015) 371–376.

[14] H.B. Li, Y.L. Ma, R. Niu, Improved capacitive deionization performance by coupling TiO_2 nanoparticles with carbon nanotubes, Sep. Purif. Technol., 171 (2016) 93–100.

[15] Z. Peng, D.S. Zhang, L.Y. Shi, T.T. Yan, High performance ordered mesoporous carbon/carbon nanotube composite electrodes for capacitive deionization, J. Mater. Chem., 22 (2012) 6603–6612.

[16] M.C. Zafra, P. Lavela, G. Rasines, C. Macías, J.L. Tirado, C.O. Ania, A novel method for metal oxide deposition on carbon aerogels with potential application in capacitive deionization of saline water, Electrochim. Acta, 135 (2014) 208–216.

[17] C. Tsouris, R. Mayes, J. Kiggans, K. Sharma, S. Yiacoumi, D. DePaoli, S. Dai, Mesoporous carbon for capacitive deionization of saline water, Environ. Sci. Technol., 45 (2011) 10243–10249.

[18] B. Milow, L. Ratke, S. Ludwig, Citric Acid Catalyzed Organic Aerogels, Proc. Seminar on Aerogels, 2012, pp. 155–165.

[19] G. Rasines, P. Lavela, C. Macías, M.C. Zafra, J.L. Tirado, J.B. Parra, C.O. Ania, N-doped monolithic carbon aerogel electrodes with optimized features for the electrosorption of ions, Carbon, 83 (2015) 262–274.

[20] M.E. Suss, T.F. Baumann, W.L. Bourcier, C.M. Spadaccini, K.A. Rose, J.G. Santiago, M. Stadermann, Capacitive desalination with flow-through electrodes, Energy Environ. Sci., 5 (2012) 9511–9519.

[21] P. Xu, J.E. Drewes, D. Heil, G. Wang, Treatment of brackish produced water using carbon aerogel-based capacitive deionization technology, Water Res., 42 (2008) 2605–2617.

[22] G.J. Doornbusch, J.E. Dykstra, P.M. Biesheuvel, M.E. Suss, Fluidized bed electrodes with high carbon loading for water desalination by capacitive deionization, J. Mater. Chem. A, 4 (2016) 3642–3647.

[23] M. Pasta, C.D. Wessells, Y. Cui, F. La Mantia, A desalination battery, Nano Lett., 12 (2012) 839–843.

[24] F. He, P.M. Biesheuvel, M.Z. Bazant, T.A. Hatton, Theory of water treatment by capacitive deionization with redox active porous electrodes, Water Res. 132 (2018) 282–291.

[25] Y.H. Liu, W. Ma, Z.H. Cheng, J. Xu, R. Wang, X. Gang, Preparing CNTs/Ca-Selective zeolite composite electrode to remove calcium ions by capacitive deionization, Desalination, 326 (2013) 109–114.

[26] G.L. Sun, H.Y. Xie, J.B. Ran, L.Y. Ma, X.Y. Shen, J.M. Hu, H. Tong, Rational design of uniformly embedded metal oxide nanoparticles into nitrogen-doped carbon aerogel for high-performance asymmetric supercapacitors with a high operating voltage window, J. Mater. Chem. A, 4 (2016) 16576–16587.

[27] X.L. Li, R.W. Tang, K. Hu, L.Y. Zhang, Z.Q. Ding, Hierarchical porous carbon aerogels with VN modification as cathode matrix for high performance lithium-sulfur batteries, Electrochim. Acta, 210 (2016) 734–742.

[28] T.F. Baumann, M.A. Worsley, T.Y.-J. Han, J.H. Satcher Jr., High surface area carbon aerogel monoliths with hierarchical porosity, J. Non-Cryst. Solids, 354 (2008) 3513–3515.

[29] R. Kumar, S. Sen Gupta, S. Katiyar, V.K. Raman, S.K. Varigala, T. Pradeep, A. Sharma, Carbon aerogels through organo-inorganic co-assembly and their application in water desalination by capacitive deionization, Carbon, 99 (2016) 375–383.

[30] C.-L. Yeh, H.-C. Hsi, K.-C. Li, C.-H. Hou, Improved performance in capacitive deionization of activated carbon electrodes with a tunable mesopore and micropore ratio, Desalination, 367 (2015) 60–68.

[31] K.B. Hatzell, M. Beidaghi, J.W. Campos, C.R. Dennison, E.C. Kumbur, Y. Gogotsi, A high performance pseudocapacitive suspension electrode for the electrochemical flow capacitor, Electrochim. Acta, 111 (2013) 888–897.

[32] Y.L. Xu, M.F. Yan, S.S. Wang, L.H. Zhang, H.H. Liu, Z.F. Liu, Synthesis, characterization and electrochemical properties of carbon aerogels using different organic acids as polymerization catalysts, J. Porous Mater., 24 (2017) 1375–1381.

[33] M.-W. Ryoo, J.-H. Kim, G. Seo, Role of titania incorporated on activated carbon cloth for capacitive deionization of NaCl solution, J. Colloid Interface Sci., 264 (2003) 414–419.

[34] X.P. Quan, Z.B. Fu, L. Yuan, M.L. Zhong, R. Mi, X. Yang, Y. Yi, C.Y. Wang, Capacitive deionization of NaCl solutions with ambient pressure dried carbon aerogel microsphere electrodes, RSC Adv., 7 (2017) 35875–35882.

[35] Z. Wang, B.J. Dou, L. Zheng, G. Zhang, Z.H. Liu, Z.P. Hao, Effective desalination by capacitive deionization with functional graphene nanocomposite as novel electrode material, Desalination, 299 (2012) 96–102.

[36] C.M. Wang, H. Song, Q.X. Zhang, B.J. Wang, A.M. Li, Parameter optimization based on capacitive deionization for highly efficient desalination of domestic wastewater biotreated effluent and the fouled electrode regeneration, Desalination, 365 (2015) 407–415.

[37] H.L. Zhang, P. Liang, Y.H. Bian, Y. Jiang, X.L. Sun, C.Y. Zhang, X. Huang, F. Wei, Moderately oxidized graphene–carbon nanotubes hybrid for high performance capacitive deionization, RSC Adv., 6 (2016) 58907–58915.

Supplementary information

Fig. S1. Copper conductive adhesive and covered the bonding areas with silicone adhesive to prevent the oxidation of the copper adhesive by air.
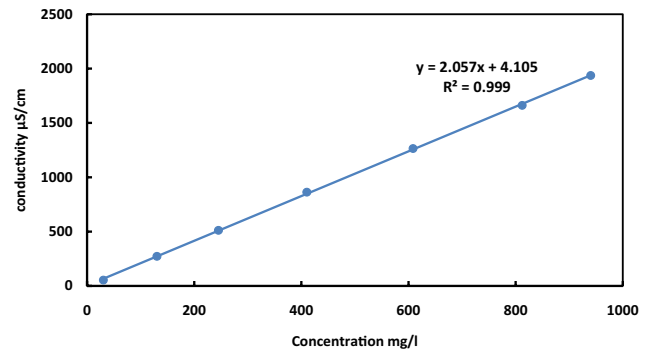
Fig. S2. NaCl solutions experimented with during this study were obtained from the equation and calibration curve.

a
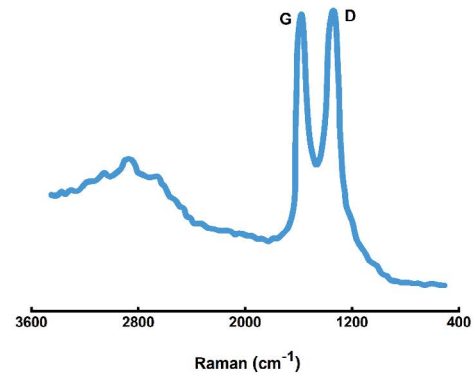
b
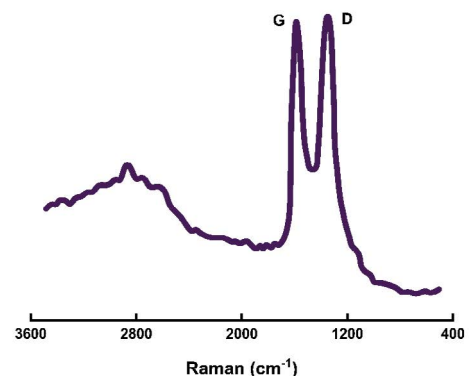
Fig. S3. Raman spectra of CA (a) and CAS (b) samples the relative intensity of the D and G band $R = I_D/I_G$ could identify the structural disorder of the sample. A higher ratio implied a perfect material. The R-values of the samples are 1.094 and 1.076 for CA and CAS, respectively. The R-value of the CA sample was higher than CAS. This result demonstrated that why CA had a larger specific area.
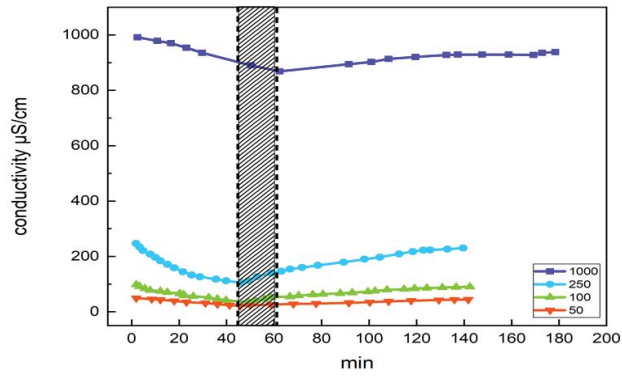
Fig. S4. Time selected for the regeneration of the electrodes at four concentrations were selected from the diagram below.
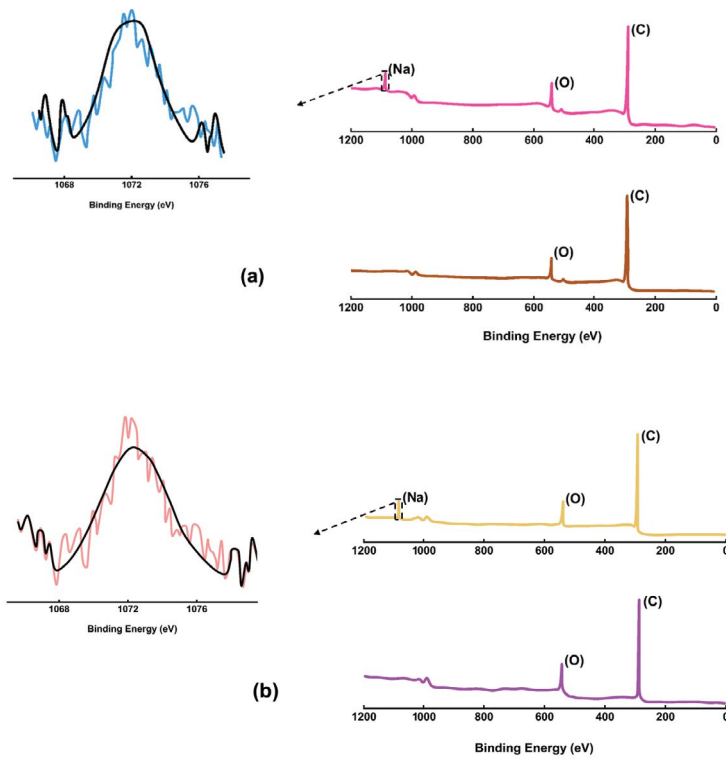
Fig. S5. X-ray photoelectron spectrum of carbon aerogels before adsorption and after adsorption of sodium in the cathode electrode: (a) CA and (b) CAS.